

---

# InTAct: Interval-based Task Activation Consolidation for Continual Learning

---

Patryk Krukowski<sup>1,2</sup> Jan Miksa<sup>1</sup> Piotr Helm<sup>1</sup> Jacek Tabor<sup>1</sup> Paweł Wawrzyński<sup>3</sup> Przemysław Spurek<sup>1,3</sup>

## Abstract

Continual learning is a fundamental challenge in artificial intelligence that requires networks to acquire new knowledge while preserving previously learned representations. Despite the success of various approaches, most existing paradigms do not provide rigorous mathematical guarantees against catastrophic forgetting. Current methods that offer such guarantees primarily focus on analyzing the parameter space using *interval arithmetic (IA)*, as seen in frameworks such as InterContiNet. However, restricting high-dimensional weight updates can be computationally expensive. In this work, we propose InTAct (Interval-based Task Activation Consolidation), a method that mitigates catastrophic forgetting by enforcing functional invariance at the neuron level. We identify specific activation intervals where previous tasks reside and constrain updates within these regions while allowing for flexible adaptation elsewhere. By ensuring that predictions remain stable within these nested activation intervals, we provide a tractable mathematical guarantee of functional invariance. We emphasize that regulating the activation space is significantly more efficient than parameter-based constraints, because the dimensionality of internal signals is much lower than that of the vast space of model weights. While our approach is architecture-agnostic and applicable to various continual learning settings, its integration with prompt-based methods enables it to achieve state-of-the-art performance on challenging benchmarks.

## 1. Introduction

Continual learning enables neural networks to acquire new knowledge over time while preserving previously learned information. Human beings naturally achieve this by main-

<sup>1</sup>Jagiellonian University <sup>2</sup>AKCES NCBR <sup>3</sup>IDEAS Research Institute. Correspondence to: Patryk Krukowski <patryk.krukowski@doctoral.uj.edu.pl>.

Preprint. February 24, 2026.

taining a balance between stability (the retention of past knowledge) and plasticity (the capacity to adapt to new tasks). Deep neural networks, however, struggle to strike this balance effectively (Kirkpatrick et al., 2017). As models adapt to new data distributions, their internal representations often undergo representational drift, modifying features that were critical for earlier tasks and leading to the phenomenon known as catastrophic forgetting (McCloskey & Cohen, 1989).

A large body of prior work addresses this issue by constraining parameter updates through regularization, architectural modifications, or optimization-based strategies (Parisi et al., 2019; De Lange et al., 2021; Masana et al., 2022). While effective to some extent, these methods predominantly operate in the parameter space and rarely provide explicit control over how the network’s function evolves across tasks. Moreover, despite the large number of continual learning strategies, most existing approaches lack rigorous mathematical guarantees against forgetting. Methods that do provide formal assurances typically rely on *interval arithmetic (IA)* in the weight space, as exemplified by frameworks such as InterContiNet (Wołczyk et al., 2022) and HINT (Krukowski et al., 2025). However, constraining high-dimensional parameter updates is computationally expensive and does not necessarily ensure the model’s functional stability.

To address these limitations, we introduce InTAct (Interval-based Task Activation Consolidation)<sup>1</sup>, a novel approach that enforces functional stability by directly regulating neural activations rather than model parameters. InTAct identifies neuron-wise activation intervals that characterize stable operating regions established during previous tasks. These intervals are aggregated at the layer level to form multidimensional hypercubes, which delineate regions of the feature space corresponding to previously acquired knowledge (see Fig. 1). During subsequent training, InTAct constrains model updates within these regions while permitting unrestricted adaptation outside them. By enforcing prediction invariance whenever internal signals remain within the preserved activation intervals, InTAct provides a tractable and efficient mathematical guarantee of functional stability.

When learning new tasks, the resulting hypercubes act as

<sup>1</sup>Code available at: <https://github.com/pkrukowski1/PromptInTAct>

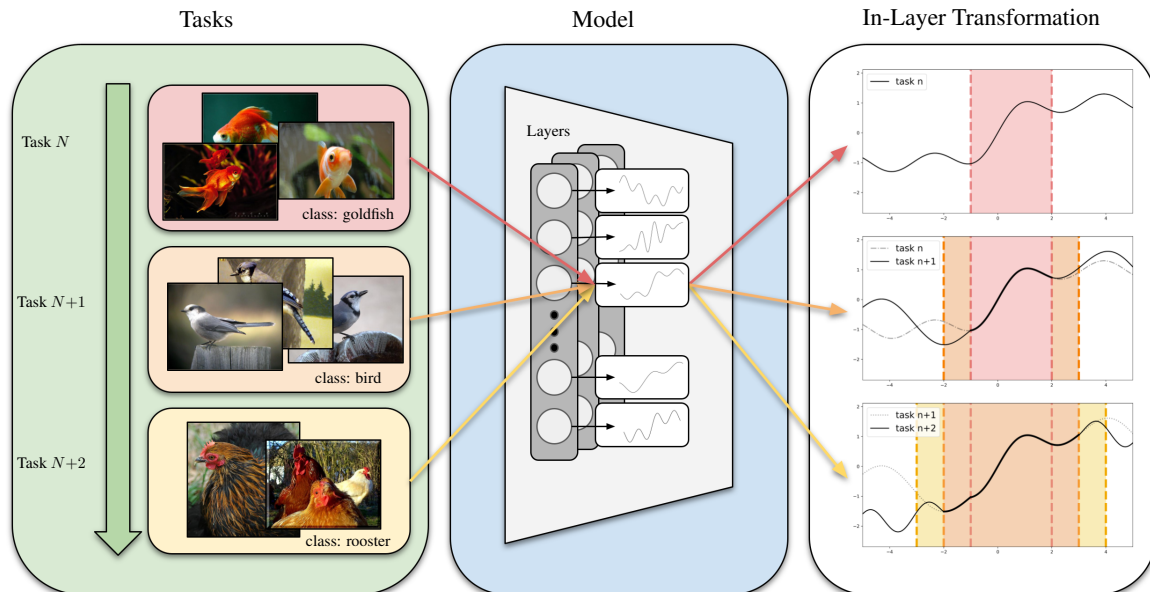


Figure 1. During training on task ( $N+1$ ), InTACT preserves the functional region established by task  $N$  (pink) while allowing the model to learn new knowledge in a distinct region (orange). After training, these regions merge into an expanded protected region (yellow), defining where the layer’s transformation should remain stable in future updates. The dashed curves illustrate transformations from earlier tasks, highlighting that their behaviors remain preserved within their respective regions, while adaptation is freely allowed outside them.

elastic boundaries: they encourage the model to remain within trusted regions for familiar concepts, while still allowing exploration beyond these regions to accommodate novel information. This mechanism naturally balances stability and plasticity. Crucially, instead of restricting the model’s parameters, InTACT directly regulates activations, which constitute the model’s observable functional behavior. This results in a more direct and effective control over how the network evolves over time.

Although the proposed framework is architecture-agnostic and applicable to a wide range of continual learning scenarios, its integration with prompt-based continual learning methods (Wang et al., 2022c;b) proves particularly effective. In this setting, InTACT achieves state-of-the-art performance on challenging domain-incremental benchmarks. Our evaluations confirm that InTACT effectively stabilizes internal representations and consistently surpasses baselines without the need for data replay or parameter regularization.

The main contributions of this work are:

1. A novel continual learning framework, InTACT, which enforces functional stability by constraining neuron activations through interval-based representations rather than parameter-level restrictions.
2. Our proposed mathematical formulation promotes stability through application of IA in the activation space,

leading to efficient and scalable continual learning.

3. InTACT seamlessly integrates with prompt-based architectures, achieving state-of-the-art performance on domain-incremental benchmarks without replay or parameter regularization.<sup>2</sup>

## 2. Related Works

For an extended overview, see Appendix A.

**Continual Learning.** Traditional strategies fall into three paradigms. *Replay-based* methods (Chaudhry et al., 2018; Buzzega et al., 2020; Uretini & Carta, 2025) store exemplars or synthetic data (Shin et al., 2017) to approximate past distributions, incurring high memory overhead. *Regularization-based* approaches (Kirkpatrick et al., 2017; Li & Hoiem, 2017; Wang et al., 2022a) constrain updates via penalties or projections to preserve knowledge but struggle with long-term stability. Finally, *Parameter-isolation* methods (Mallya & Lazebnik, 2018; Serrà et al., 2018; Liang & Li, 2024b) utilize task-specific subspaces but often require restrictive task IDs during inference.

**Prompt-Based Continual Learning.** Recent architectures leverage frozen pre-trained backbones, directing adap-

<sup>2</sup>Integration details are provided in Appendix J.

tation via learnable prompts. L2P (Wang et al., 2022c) and DualPrompt (Wang et al., 2022b) utilize a pool of keys and prompts to query task-specific knowledge. Works like CODA-Prompt (Smith et al., 2023) enhance this via attention-based decomposition, while C-Prompt (Liu et al., 2024) focuses on inter-task consistency. Despite their success, these methods remain vulnerable to *representational drift* in shared components, specifically the prompt keys and the classification head. This drift is especially detrimental in Domain-Incremental Learning (DIL), where task boundaries are inherently ambiguous.

**Interval Arithmetic in Continual Learning.** While interval arithmetic (IA) (Dahlquist & Björck, 2008; Moore et al., 2009) provides attractive possibilities for obtaining rigorous numerical bounds in theory, its adoption in continual learning remains largely underexplored. Existing approaches primarily apply IA to constrain the *parameter space*. For instance, InterContiNet (Wołczyk et al., 2022) isolates safe intervals for weights to ensure multi-task compatibility, while HINT (Krukowski et al., 2025) utilizes hypernetworks to map interval-based embeddings to network parameters. However, full interval propagation through deep networks is notoriously susceptible to the *wrapping effect* (Moore et al., 2009), where error bounds expand exponentially with depth, leading to overly loose constraints. In contrast, InTAct circumvents this issue by avoiding interval propagation altogether. Instead, we employ IA locally to define static *hypercubes* that encapsulate the geometric bounds of prior task data. By regularizing representations to remain within these pre-calculated bounds, we ensure functional stability without the computational overhead or bound-explosion associated with traditional interval propagation.

### 3. Method

Continual learning requires a model to learn new tasks without forgetting previous ones. Prompting methods, such as CODA-Prompt, optimize small sets of learnable parameters to steer a frozen backbone’s representations, a paradigm we describe in detail in Appendix B. However, even with a frozen backbone, the shared classifier and the prompt pool itself remain highly vulnerable to drift as new tasks are added. We introduce InTAct to stabilize both components. Specifically, we enforce a condition where the classifier produces the same predictions for any point within protected feature regions. Simultaneously, we stabilize the prompts to ensure they continue to produce the same [CLS] tokens for historical data. This dual control ensures the model maintains consistent behavior and navigation across its entire latent space as it integrates new tasks.

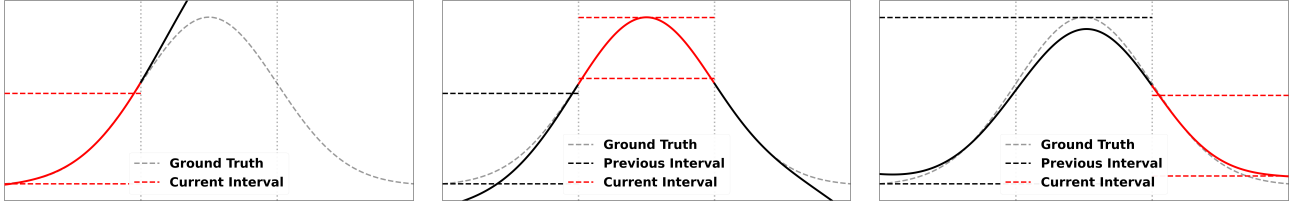
**Core Mechanism.** We analyze prompt-based architectures (e.g., ViT (Dosovitskiy et al., 2021)), where classification relies on a summary vector, typically the [CLS] token. To prevent forgetting, decision boundaries must remain stable within the feature space regions occupied by previous tasks. While probabilistic estimators like Gaussian Mixture Models (GMMs) approximate these regions, they provide soft likelihoods rather than the hard limits required for formal guarantees. Consequently, we compute deterministic *bounding boxes (hypercubes)* that tightly enclose the stable support of these task-specific representations.

These hypercubes act as protected zones in the feature space. InTAct enforces two conditions to maintain stability: first, the classifier must yield consistent predictions for every point within a hypercube, creating a stable decision region rather than just protecting discrete points. Second, we stabilize the prompts to ensure they continue to map old data to consistent summary embeddings. By utilizing hypercubes, we leverage IA to mathematically verify entire regions at once, preserving knowledge of previous tasks while allowing adaptation in unoccupied space.

**Conceptual Visualization.** To illustrate how InTAct works, Fig. 2 shows a 1D example in which the model must continually learn three distinct segments of a Gaussian function. In Task 1, the model learns the first segment, and InTAct calculates a “safe zone” (a 1D hypercube) to protect it. When the model learns the central peak in Task 2, our method prevents any changes to the output within that first safe zone. This ensures the model learns the new peak without erasing the previously learned segment. Finally, in Task 3, the model learns the third segment while both previous zones remain protected. Although simple, this 1D example mirrors our high-dimensional approach: hypercubes act as anchors that only allow the model to change in areas that do not interfere with old knowledge.

#### 3.1. Activation Interval Representation

To preserve stability without the memory cost of replay buffers, we construct a compact geometric abstraction of the feature distribution. Below, we provide a general formulation for constructing a hypercube for a single layer. In our specific implementation, we apply this mechanism to the [CLS] token representations and the internal classifier layers. For these target regions, we identify the active range in which each individual neuron responds to a task’s data. We define an **interval** for each neuron, representing a single dimension of the hypercube, which captures its specific stable activation range. Collectively, these intervals map out a “safe zone”, a high-dimensional hypercube, for the entire representation.



(a) Task 1: Initial learning and interval computation.

(b) Task 2: Adaptation with stability constraints.

(c) Task 3: Global accumulation without forgetting.

**Figure 2. Toy Example.** We train a model to approximate a Gaussian function over three sequential tasks. The shaded bands represent the **hypercubes** (1D intervals) computed by InTAct after each task. In the subsequent steps (b, c), these intervals act as **anchors**: they strictly enforce stability in the regions occupied by prior tasks while allowing the function to evolve freely in new, unoccupied spaces (plasticity).

**Hypercube Construction.** For a selected layer, let  $\mathbf{x}_t \in \mathbb{R}^d$  denote the feature representation (such as the [CLS] token or a hidden classifier feature) derived from the training data of task  $t$ . To ensure these boundaries are robust against outliers, we approximate the data distribution using a quantile-based bounding box. Specifically, we capture the central  $p\%$  of the activations, filtering out the extreme tails defined by  $\alpha = \frac{100-p}{2}\%$ .

Before the data for task  $t$  is removed from memory, we perform a final inference pass to establish the bounds for each neuron  $j$ :

$$\mathcal{H}_t[j] = [\underline{x}_t[j], \bar{x}_t[j]], \quad (1)$$

where  $\underline{x}$  and  $\bar{x}$  are the  $\alpha$ -th and  $(100 - \alpha)$ -th percentiles. This statistical clipping ensures that the constraints focus on the dense, meaningful regions of the feature space rather than sparse outliers.

**Cumulative Knowledge Aggregation.** To respect the constraints of all previous tasks without storing their data, we maintain a single cumulative hypercube  $\mathcal{H}^{(\leq t)}$ . This acts as a “convex hull” that grows to encompass all historical safe zones. After completing task  $t$ , we update the global boundary by merging the new task-specific intervals with the existing historical bounds:

$$\mathcal{H}^{(\leq t)} = \left[ \min(\underline{x}^{(t-1)}, \underline{x}_t), \max(\bar{x}^{(t-1)}, \bar{x}_t) \right]. \quad (2)$$

This operation computes the smallest hypercube that contains the entire history of the past representations. While this approach may include some unoccupied space between task clusters, it ensures that the memory footprint remains constant ( $O(1)$ ) regardless of the number of tasks. This provides a highly efficient and scalable mechanism for checking stability during all future training phases.

### 3.2. Functional Preservation via Regularization

In this subsection, we detail our strategy for protecting the classifier and stabilizing the prompts. First, we describe how to regularize the classifier’s layers. By calculating

the hypercube around the [CLS] token, we can provide a formal mathematical guarantee: in the limit where our drift loss is minimized to zero, the classifier’s output is guaranteed to remain unchanged for any point within that protected region. Second, we describe how to stabilize the prompts. This ensures the frozen backbone continues to produce the same representations for old data, keeping them anchored within the safe zones where the classifier’s behavior is fixed.

**Internal Representation Drift Loss.** For clarity and without loss of generality, we describe our approach focusing on a single affine layer within the classifier head, though the formulation extends naturally to multi-layer architectures. Let  $f(\cdot; \theta)$  represent this shared classifier head,  $\theta = \langle W, b \rangle$ , parameterized by weights  $W$  and bias  $b$ . Let  $\mathcal{H}_{[\text{CLS}]}^{(\leq t-1)}$  denote the cumulative hypercube bounding the [CLS] token representations, denoted as  $\mathbf{z}$ , observed up to task  $t - 1$ .

When training on a new task  $t$ , the classifier parameters evolve from  $\{W, b\}$  to  $\{W + \Delta W, b + \Delta b\}$ . To prevent catastrophic forgetting, we must ensure that this parameter shift does not distort the model’s output for any latent vector  $\mathbf{z}$  residing within the established “safe zones” of prior tasks. Ideally, the functional behavior should satisfy:

$$f(\mathbf{z}; \theta + \Delta\theta) \approx f(\mathbf{z}; \theta), \quad \forall \mathbf{z} \in \mathcal{H}_{[\text{CLS}]}^{(\leq t-1)}. \quad (3)$$

Because the final class prediction is determined by a softmax operation, we only need to keep the values immediately preceding it (the logits) stable to ensure the model’s output remains unchanged. We define the classifier’s output for a representation  $\mathbf{z}$  as  $f(\mathbf{z}) = W\mathbf{z} + b$ . When we update the parameters from  $(W, b)$  to  $(W', b')$ , the shift in the model’s logic is the difference between the new and old outputs:

$$\text{Drift}(\mathbf{z}) = (W'\mathbf{z} + b') - (W\mathbf{z} + b) = \Delta W\mathbf{z} + \Delta b, \quad (4)$$

where  $\Delta W$  and  $\Delta b$  represent the changes made during the current training task. Our goal is not to strictly force this drift to zero (which would prevent the model from learning anything new), but to minimize its maximum possible magnitude across the entire hypercube volume. This formulation allows us to use interval arithmetic (IA) to calculate

an upper bound on how much the model’s ”memory” can shift within our safe zones.

**Tractability via Interval Arithmetic.** Enforcing the stability constraint in Eq. (4) pointwise is intractable, as the hypercube  $\mathcal{H}_{[\text{CLS}]}^{(\leq t-1)}$  contains an infinite number of latent vectors. Standard sampling methods fail to guarantee stability in unsampled regions, potentially leaving ”blind spots” where catastrophic forgetting can occur. To overcome this, we employ IA to compute a rigorous upper bound on the functional drift over the *entire geometric region* simultaneously. By treating the hypercube as a vector of intervals  $\mathcal{H}^{(\leq t-1)} = [\underline{\mathbf{z}}, \bar{\mathbf{z}}]$  (we omit the layer and task indices to simplify the notation), we compute the worst-case output deviation induced by parameter updates. Importantly, IA provides formal mathematical guarantees: in the limit where the drift bound is constrained to zero, the model is guaranteed to exhibit zero forgetting across the entire previously occupied feature space.

For the  $i$ -th output unit, let  $\Delta \mathbf{w}_i$  denote the  $i$ -th row of the weight update matrix. We decompose this vector into its positive and negative components:  $(\Delta \mathbf{w}_i)^+ = \max(\Delta \mathbf{w}_i, 0)$  and  $(\Delta \mathbf{w}_i)^- = \max(-\Delta \mathbf{w}_i, 0)$ . The exact bounds of the output drift,  $[\tilde{y}_i, \bar{y}_i]$ , are then given by:

$$\tilde{y}_i = (\Delta \mathbf{w}_i)^+ \underline{\mathbf{z}} - (\Delta \mathbf{w}_i)^- \bar{\mathbf{z}} + \Delta b_i, \quad (5)$$

$$\bar{y}_i = (\Delta \mathbf{w}_i)^+ \bar{\mathbf{z}} - (\Delta \mathbf{w}_i)^- \underline{\mathbf{z}} + \Delta b_i. \quad (6)$$

This formulation (derived in Appendix G) guarantees that we capture the worst-case deviation.

We define the internal representation drift loss ( $\mathcal{L}_{\text{IntDrift}}$ ) to minimize the worst-case magnitude of these deviations. Let  $N$  be the number of output units (e.g., classes). By driving the squared bounds to zero, weighted by a coefficient  $\lambda_{\text{IntDrift}}$ , we ensure that the classifier’s output remains invariant for *any* input  $\mathbf{z}$  within the protected region:

$$\mathcal{L}_{\text{IntDrift}} = \frac{\lambda_{\text{IntDrift}}}{N} \sum_{i=1}^N \left( (\tilde{y}_i)^2 + (\bar{y}_i)^2 \right). \quad (7)$$

**Comparison to Existing Regularizers.** Standard parameter-based methods (e.g., EWC, SI) mitigate forgetting by restricting changes to the *weights* themselves. However, preserving weights is merely a proxy for preserving stability. In contrast,  $\mathcal{L}_{\text{IntDrift}}$  constrains the model’s *outputs* directly. This distinction is critical: our method permits significant changes to the parameters, provided those updates do not alter the representations of protected inputs. By decoupling ”weight rigidity” from ”functional stability,” we grant the optimization process much greater freedom to accommodate new tasks without breaking old ones. Furthermore, unlike replay-based methods that rely

on storing raw images, our approach substitutes data buffers with lightweight geometric bounds (hypercubes). This resolves the privacy risks of archiving user data and ensures that memory usage scales with the feature dimension rather than the dataset size.

**Note on Prompt-Classifier Interdependence.** The stability of the classifier depends entirely on the representation  $\mathbf{z}$  staying within its protected hypercube. However, because the prompts are learnable, updates for new tasks can accidentally push the [CLS] tokens of old data outside these fixed safe zones. If the embeddings ”escape” their boxes, our regularization no longer applies. To prevent this, we regularize the prompts to ensure they continue to steer old data into the same protected regions. Essentially, we anchor the prompts so that historical inputs are still mapped into the cumulative hypercube where the classifier’s logic has already been locked.

**Prompt-Dependent Feature Stability.** To prevent prompt updates from steering old data out of their safe zones, we employ a region-selective distillation loss. We define a binary gating function  $w(\mathbf{z})$  that identifies if a representation falls within the cumulative hypercube:

$$w(\mathbf{z}^{(t-1)}) = \mathbb{I} \left[ \mathbf{z}^{(t-1)} \in \mathcal{H}^{(\leq t-1)} \right], \quad (8)$$

where  $\mathbb{I}[\cdot]$  is the indicator function. The feature stability Loss ( $\mathcal{L}_{\text{Feat}}$ ) then enforces consistency between the current representation (Student) and the previous snapshot (Teacher) only when this gate is active:

$$\mathcal{L}_{\text{Feat}} = \frac{\lambda_{\text{Feat}}}{N_B} \sum_{i=1}^{N_B} w(\mathbf{z}_i^{(t-1)}) \cdot \left\| \mathbf{z}_i^{(t)} - \mathbf{z}_i^{(t-1)} \right\|_2^2. \quad (9)$$

This ensures that the prompts maintain the original input-to-feature transformation for samples recognized as belonging to prior tasks, while remaining fully plastic ( $w = 0$ ) to adapt to novel data distributions.

**Compactness Regularization.** The effectiveness of InTAct depends on the volume of the hypercubes. If the [CLS] tokens for a task are widely scattered in the feature space, the resulting hypercube will be too large. This leads to loose mathematical bounds and increases the chance that new tasks will accidentally overlap with old ”safe zones.”

To prevent this, we use  $\mathcal{L}_{\text{Var}}$  to enforce *intra-task compactness*. This loss forces the representations of the current task to cluster tightly together. Let  $\mathbf{z}_i$  denote the [CLS] token for the  $i$ -th sample in a mini-batch of size  $N_B$ . We compute the batch centroid  $\bar{\mathbf{z}}^{(t)}$  as:

$$\bar{\mathbf{z}}^{(t)} = \frac{1}{N_B} \sum_{i=1}^{N_B} \mathbf{z}_i. \quad (10)$$

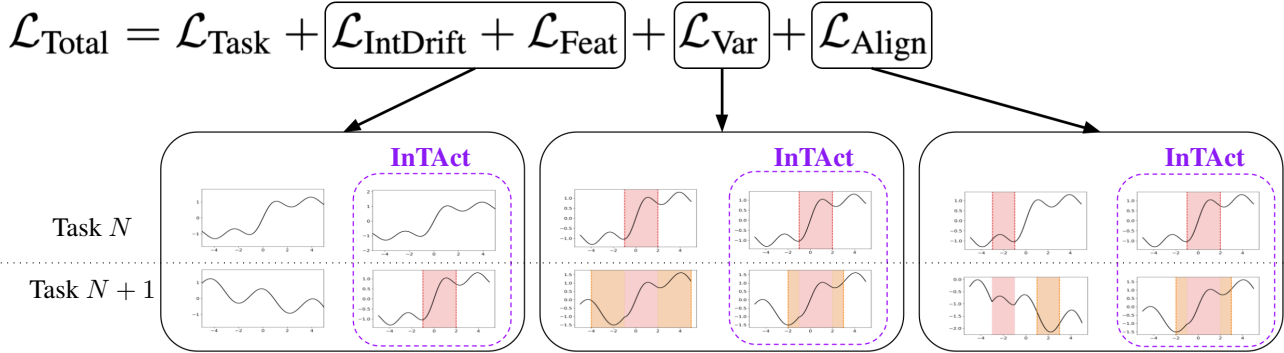


**Figure 3. InTACT Regularization Overview.** (Left)  $\mathcal{L}_{\text{IntDrift}}$  and  $\mathcal{L}_{\text{Feat}}$  enforce functional invariance for inputs within the **protected hypercubes** (Pink). (Center)  $\mathcal{L}_{\text{Var}}$  minimizes the intra-task variance of **new activation regions** (Orange), constraining their volume. (Right)  $\mathcal{L}_{\text{Align}}$  penalizes the distance between task centroids to limit the expansion of the cumulative boundary. **Purple outlines** illustrate the stabilized, compact geometry achieved by InTACT.

The variance penalty is then the mean squared distance from this centroid:

$$\mathcal{L}_{\text{Var}} = \frac{\lambda_{\text{Var}}}{N_B} \sum_{i=1}^{N_B} \left\| \mathbf{z}_i - \bar{\mathbf{z}}^{(t)} \right\|_2^2. \quad (11)$$

By minimizing this loss, we compress the feature distribution. This results in tighter hypercube bounds, ensuring that our stability guarantees are strictly localized and do not interfere with the model’s ability to learn future tasks.

**Convex Hull Volume Minimization.** Using a single cumulative hypercube  $\mathcal{H}^{(\leq t)}$  can lead to excessive volume expansion if new task representations drift far from historical ones. This creates overly restrictive regions in unoccupied feature space, limiting future plasticity. To mitigate this, we introduce  $\mathcal{L}_{\text{Align}}$ , which encourages new task [CLS] tokens to reside near existing bounds without merging classes.

We define the geometric center  $\mathbf{c}$  and average radius  $r$  of a task’s safe zone as:

$$\mathbf{c} = \frac{\mathbf{z} + \bar{\mathbf{z}}}{2}, \quad r = \text{mean} \left( \frac{\bar{\mathbf{z}} - \mathbf{z}}{2} \right). \quad (12)$$

The alignment loss penalizes the distance between the new task center  $\mathbf{c}_t$  and the historical center  $\mathbf{c}_{t-1}$ , scaled by the previous manifold’s breadth:

$$\mathcal{L}_{\text{Align}} = \lambda_{\text{Align}} \frac{\left\| \mathbf{c}_t - \mathbf{c}_{t-1} \right\|_2^2}{r_{t-1} + \varepsilon}. \quad (13)$$

By scaling the penalty by  $r_{t-1}$ , we enforce compact representations that align with the existing task geometry. This ensures efficient hypercube growth and preserves plasticity by minimizing unnecessary constraints on unoccupied feature space.

**Composite Training Objective.** Our final optimization target synthesizes the task-specific learning objective with

the proposed stability and architectural constraints. The total loss function is formulated as:

$$\mathcal{L}_{\text{Total}} = \mathcal{L}_{\text{CE}} + \underbrace{\mathcal{L}_{\text{IntDrift}} + \mathcal{L}_{\text{Feat}}}_{\text{Functional Stability}} + \underbrace{\mathcal{L}_{\text{Var}} + \mathcal{L}_{\text{Align}}}_{\text{Representation Structuring}}. \quad (14)$$

Here,  $\mathcal{L}_{\text{CE}}$  denotes the standard Cross-Entropy loss for the current task. The remaining terms are weighted by scalar coefficients to ensure that the structural constraints do not overwhelm the primary learning objective. Specifically, the *Functional Stability* terms lock the model’s logic for old data. Simultaneously, the *Representation Structuring* terms ensure that the activations (both the [CLS] tokens and the hidden classifier features) are organized compactly. The structural interplay between these components is illustrated in Fig. 3, and the detailed training procedure is provided in Appendix 1.

## 4. Experiments

We evaluate InTACT in the DIL setting, focusing on three key areas: comparative performance against state-of-the-art methods, plasticity under distribution shifts, and the individual contribution of each loss component to the stability-plasticity trade-off.

### 4.1. Experimental Setup

**Datasets and Baselines.** We evaluate InTACT across four benchmarks: DomainNet, ImageNet-R, ImageNet-C, and ImageNet-Mix. We compare performance against classical baselines (EWC, LwF) and state-of-the-art approaches (L2P, DualPrompt, CODA-Prompt, KA-Prompt, InfLoRA), with a particular emphasis on prompt-based methods. The formal definition of AA is provided in Appendix F.

**Implementation.** Full implementation details and hyperparameter configurations are provided in Appendix C.

**Table 1. Benchmarking against the State-of-the-Art.** We report AA across four diverse DIL benchmarks as the mean over three runs. InTAct achieves the highest average performance, substantially outperforming existing methods on ImageNet-R and ImageNet-Mix. On DomainNet and ImageNet-C, InTAct remains highly competitive, either matching or closely approaching the best results. Presented results are achieved by integrating InTAct into CODA-Prompt. Baseline results are sourced from (Xu et al., 2025).

Method	Ref.	DomainNet	ImageNet-R	ImageNet-C	ImageNet-Mix	Average
EWC	<i>PNAS 2017</i>	47.10±0.58	51.83±0.33	65.20±1.23	57.82±0.90	55.49±0.42
LwF	<i>T-PAMI 2017</i>	54.85±0.06	57.11±0.95	69.01±1.21	65.27±0.93	61.56±0.45
L2P	<i>CVPR 2022</i>	53.74±0.04	56.55±0.33	77.86±0.44	64.20±0.34	63.09±0.16
S-Prompts	<i>NeurIPS 2022</i>	44.08±0.05	27.23±0.16	60.25±0.28	24.25±0.19	38.95±0.09
DualPrompt	<i>ECCV 2022</i>	55.18±0.02	59.47±1.00	78.52±0.30	63.57±0.17	64.19±0.26
ESN	<i>AAAI 2023</i>	45.74±0.25	16.39±0.23	68.34±0.39	14.99±0.53	36.37±0.19
CODA-P	<i>CVPR 2023</i>	55.81±0.03	55.21±0.33	78.25±0.16	64.92±0.04	63.55±0.09
InfLoRA	<i>CVPR 2024</i>	48.76±0.30	41.20±1.65	53.12±0.16	35.38±0.27	44.62±0.43
Cprompt	<i>CVPR 2024</i>	52.88±0.12	59.48±1.09	70.08±0.07	63.64±0.74	61.52±0.33
C-Prompt	<i>IJCV 2024</i>	58.66±0.05	62.43±0.49	79.84±0.38	65.35±0.52	66.57±0.20
KA-Prompt	<i>ICML 2025</i>	<b>62.91±0.14</b>	<u>66.51±0.36</u>	<u>85.43±0.56</u>	<u>70.35±0.32</u>	<u>71.30±0.19</u>
<b>InTAct</b>	<i>This Paper</i>	56.66±0.39	<b>74.23±0.16</b>	<b>85.85±0.34</b>	<b>74.20±0.28</b>	<b>72.74±0.10</b>

## 4.2. Results

**Main Results.** Table 1 reports the AA across four DIL benchmarks. Overall, InTAct achieves the highest average performance among all compared methods. In particular, InTAct sets a new state-of-the-art on ImageNet-R and ImageNet-Mix, outperforming the strongest baseline, KA-Prompt, by approximately **7.7 p.p.** and **4 p.p.**, respectively. On DomainNet and ImageNet-C, InTAct remains competitive, closely matching or slightly exceeding prior best results.

These results highlight the limitations of parameter-space regularization under substantial domain shifts, as such methods often fail to account for how weight updates propagate into destabilizing fluctuations in feature space. In contrast, InTAct leverages IA and targeted regularization to directly stabilize representations produced by the feature extractor, preserving knowledge of previously learned tasks while maintaining sufficient latent capacity for future adaptation. On corruption-prone benchmarks such as ImageNet-C and ImageNet-Mix, where input perturbations typically reduce performance, InTAct maintains high robustness. This suggests that InTAct establishes stable decision regions that are less sensitive to noise, enabling the model to produce reliable outputs even under significant distribution shifts.

**AA Evolution Analysis on ImageNet-R.** Fig. 4 illustrates the evolution of AA on the ImageNet-R benchmark over 15 tasks. As shown, InTAct establishes a new state-of-the-art, consistently surpassing the nearest competitors by a significant margin throughout the continual learning process. While baselines such as EWC and LwF experience a sharp performance decline at the 9-th task, InTAct maintains a robust trajectory with minimal degradation. Further-

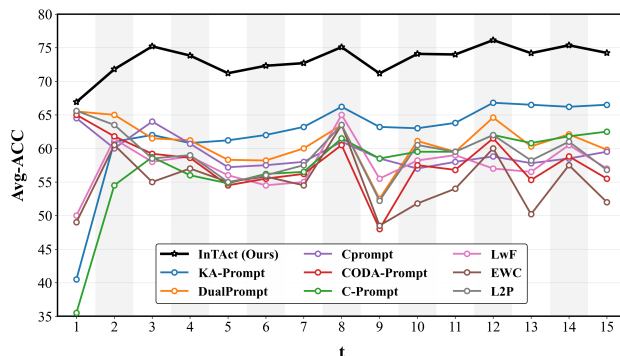


**Figure 4. AA Evolution on ImageNet-R.** Above plot reports the AA across 15 incremental tasks. InTAct (black line with stars) consistently outperforms state-of-the-art prompt-based baselines (e.g., KA-Prompt, DualPrompt) and regularization methods (e.g., EWC, LwF). Notably, our method demonstrates superior stability, maintaining high accuracy even during challenging task transitions (e.g.,  $t = 9$ ) where other methods exhibit significant forgetting. Baseline results are sourced from (Xu et al., 2025).

more, compared to recent prompt-based approaches like KA-Prompt and C-Prompt, InTAct exhibits a more favorable plasticity-stability trade-off, concluding with a final AA of roughly 75%, whereas the closest baselines finish below 67%.

## 4.3. Ablation Study

To verify the necessity of each component in the InTAct method, we conduct a systematic ablation study on the ImageNet-R benchmark (Table 2). We remove one loss term at a time to isolate its specific contribution to the stability-plasticity dynamics.

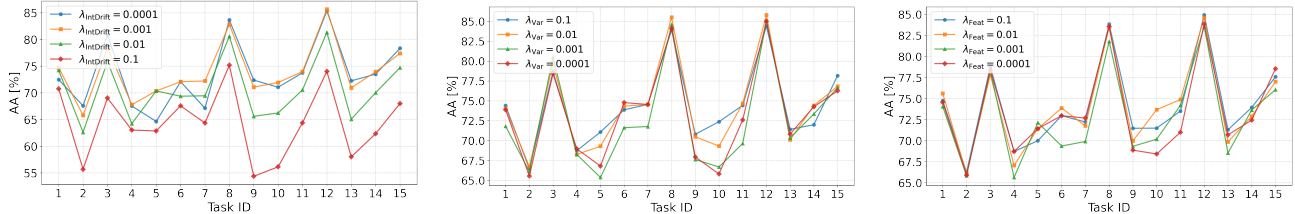
(a) Sensitivity to  $\lambda_{\text{IntDrift}}$  changes(b) Sensitivity to  $\lambda_{\text{Var}}$  changes(c) Sensitivity to  $\lambda_{\text{Feat}}$  changes

Figure 5. Hyperparameter sensitivity on ImageNet-R reflected by AA evolution averaged over two independent runs. (a) Lower drift penalties allow necessary classifier plasticity. (b) Stronger variance regularization improves stability by enforcing compact representations. (c) High feature stability strength is critical for preventing the backbone’s output drift.

Table 2. **Ablation Study.** Impact of removing individual loss components on ImageNet-R. We report the performance drop ( $\Delta$ ) relative to the baseline InTAct. Results are averaged over 2 random seeds.

$\mathcal{L}_{\text{IntDrift}}$	$\mathcal{L}_{\text{Var}}$	$\mathcal{L}_{\text{Align}}$	$\mathcal{L}_{\text{Feat}}$	AA (%)	$\Delta$
✓	✓	✓	✓	<b>74.23</b>	—
×	✓	✓	✓	70.75	-3.48
✓	×	✓	✓	73.28	-0.95
✓	✓	×	✓	73.76	-0.47
✓	✓	✓	×	72.44	-1.79

The empirical results confirm that the full set of regularization terms is essential for optimal performance. The exclusion of the core interval drift loss term ( $\mathcal{L}_{\text{IntDrift}}$ ) results in the most severe degradation, lowering AA by **3.48** p.p. These findings support our central hypothesis that interval-based constraints are the key mechanism for preserving representations across domain shifts. The feature stability loss ( $\mathcal{L}_{\text{Feat}}$ ) is also crucial: removing it results in a **1.79** p.p. drop in performance, underscoring the importance of anchoring general feature representations.

Removing the compactness penalty ( $\mathcal{L}_{\text{Var}}$ ) lowers AA by **0.95** p.p. because, without it, representations from the backbone expand and cause inter-task overlap. Similarly, removing the alignment term ( $\mathcal{L}_{\text{Align}}$ ) leads to a **0.47** p.p. decrease. This shows that alignment is necessary to keep the cumulative hypercube tight, preventing features from drifting into “dead zones” that waste the limited capacity of the prompt pool.

#### 4.4. Sensitivity Analysis on ImageNet-R

We investigate the sensitivity of InTAct to its regularization hyperparameters on ImageNet-R.

**Internal Drift Regularization ( $\lambda_{\text{IntDrift}}$ ).** As shown in Fig. 5a, lower  $\lambda_{\text{IntDrift}}$  values yield significantly higher accuracy, while strong penalties degrade performance. This indicates that the classifier requires plasticity to adapt to the large stylistic shifts in ImageNet-R. Excessive regularization

overly constrains decision boundary updates, preventing effective adaptation.

**Variance Regularization ( $\lambda_{\text{Var}}$ ).** As shown in Fig. 5b, increasing  $\lambda_{\text{Var}}$  mitigates performance drops by encouraging compact feature clusters for each learned task. By minimizing the latent volume occupied by current representations, this term reduces inter-task interference and preserves available capacity for the plastic adaptation of subsequent tasks.

**Feature Stability ( $\lambda_{\text{Feat}}$ ).** As shown in Fig. 5c, higher  $\lambda_{\text{Feat}}$  values are essential for maintaining stability throughout the task sequence. This loss encourages the model to maintain established mappings at both the backbone and prompt level for previous tasks. By ensuring that inputs are consistently mapped into their respective hypercubes, InTAct prevents new task adaptation from overwriting old knowledge, effectively mitigating representational drift while preserving the integrity of the feature space.

## 5. Conclusion

We introduced InTAct, a continual learning framework that addresses catastrophic forgetting by regulating functional behavior rather than constraining individual parameters. Through IA, the method imposes regularization that preserves model outputs within the regions corresponding to previously learned tasks. This design cleanly separates stability from plasticity: the model remains stable where prior knowledge is encoded, yet retains full adaptability in unconstrained regions of the representation space. Extensive experiments demonstrate that InTAct consistently strengthens existing prompt-based approaches, achieving state-of-the-art performance in the DIL setting without relying on data replay or architectural growth.

**Limitations.** While our framework is currently integrated into CODA-Prompt, extending it to more recent approaches such as KA-Prompt could yield further performance gains; however, we encountered challenges in reproducing the reported KA-Prompt results.

## References

- Aljundi, R., Babiloni, F., Elhoseiny, M., Rohrbach, M., and Tuytelaars, T. Memory aware synapses: Learning what (not) to forget, 2018. URL <https://arxiv.org/abs/1711.09601>.
- Buzzega, P., Boschini, M., Porrello, A., Abati, D., and Calderara, S. Dark experience for general continual learning: a strong, simple baseline. In *Advances in neural information processing systems*, volume 33, pp. 15920–15930, 2020.
- Chaudhry, A., Ranzato, M., Rohrbach, M., and Elhoseiny, M. Efficient lifelong learning with a-gem. In *International Conference on Learning Representations*, 2018.
- Chaudhry, A., Rohrbach, M., Elhoseiny, M., Ajanthan, T., Dokania, P. K., Torr, P. H. S., and Ranzato, M. On tiny episodic memories in continual learning, 2019. arXiv preprint arXiv:1902.10486.
- Chen, Z., Wuerkaixi, A., Cui, S., Li, H., Li, D., Zhang, J., Han, B., Niu, G., Liu, H., Yang, Y., Yang, S., Zhang, C., and Ren, T. Learning without isolation: Pathway protection for continual learning. In *International Conference on Machine Learning*, 2025.
- Dahlquist, G. and Björck, Å. *Numerical methods in scientific computing, volume 1*. SIAM, 2008.
- De Lange, M., Aljundi, R., Masana, M., Parisot, S., Jia, X., Leonardis, A., Slabaugh, G., and Tuytelaars, T. A continual learning survey: Defying forgetting in classification tasks. *IEEE transactions on pattern analysis and machine intelligence*, 44(7):3366–3385, 2021.
- Dosovitskiy, A., Beyer, L., Kolesnikov, A., Weissenborn, D., Zhai, X., Unterthiner, T., Dehghani, M., Minderer, M., Heigold, G., Gelly, S., Uszkoreit, J., and Houlsby, N. An image is worth 16x16 words: Transformers for image recognition at scale, 2021. URL <https://arxiv.org/abs/2010.11929>.
- Gao, Z., Cen, J., and Chang, X. Consistent prompting for rehearsal-free continual learning. In *Proceedings of the IEEE/CVF Conference on Computer Vision and Pattern Recognition*, pp. 28463–28473, 2024.
- Goswami, D., Liu, Y., Twardowski, B., and van de Weijer, J. Fecam: Exploiting the heterogeneity of class distributions in exemplar-free continual learning, 2024a. URL <https://arxiv.org/abs/2309.14062>.
- Goswami, D., Soutif-Cormerais, A., Liu, Y., Kamath, S., Twardowski, B., and van de Weijer, J. Resurrecting old classes with new data for exemplar-free continual learning. In *Proceedings of the IEEE/CVF Conference on Computer Vision and Pattern Recognition*, pp. 28525–28534, 2024b.
- Hendrycks, D. and Dietterich, T. G. Benchmarking neural network robustness to common corruptions and surface variations, 2019. URL <https://arxiv.org/abs/1807.01697>.
- Hendrycks, D., Basart, S., Mu, N., Kadavath, S., Wang, F., Dorundo, E., Desai, R., Zhu, T., Parajuli, S., Guo, M., Song, D., Steinhardt, J., and Gilmer, J. The many faces of robustness: A critical analysis of out-of-distribution generalization. *ICCV*, 2021.
- Janson, P., Zhang, W., Aljundi, R., and Elhoseiny, M. A simple baseline that questions the use of pretrained-models in continual learning. In *NeurIPS 2022 Workshop on Distribution Shifts: Connecting Methods and Applications*, 2022.
- Jaulin, L., Kieffer, M., Didrit, O., and Walter, E. *Applied Interval Analysis: With Examples in Parameter and State Estimation, Robust and Control*. Springer, London, 2001. doi: 10.1007/978-1-4471-0249-6.
- Kim, S., Noci, L., Orvieto, A., and Hofmann, T. Achieving a better stability-plasticity trade-off via auxiliary networks in continual learning. In *Proceedings of the IEEE/CVF Conference on Computer Vision and Pattern Recognition*, pp. 11930–11939, 2023.
- Kirkpatrick, J., Pascanu, R., Rabinowitz, N., Veness, J., Desjardins, G., Rusu, A. A., Milan, K., Quan, J., Ramalho, T., Grabska-Barwinska, A., Hassabis, D., Clopath, C., Kumaran, D., and Hadsell, R. Overcoming catastrophic forgetting in neural networks. *Proceedings of the National Academy of Sciences*, 114(13):3521–3526, March 2017. ISSN 1091-6490. doi: 10.1073/pnas.1611835114. URL <http://dx.doi.org/10.1073/pnas.1611835114>.
- Kong, Y., Liu, L., Wang, Z., and Tao, D. Balancing stability and plasticity through advanced null space in continual learning. In *European Conference on Computer Vision*, pp. 219–236, 2022.
- Krukowski, P., Bielawska, A., Ksiazek, K., Wawrzyński, P., Batorski, P., and Spurek, P. Hint: Hypernetwork approach to training weight interval regions in continual learning. *Information Sciences*, 717:122261, 2025.
- Li, X. L. and Liang, P. Prefix-tuning: Optimizing continuous prompts for generation, 2021. URL <https://arxiv.org/abs/2101.00190>.
- Li, Z. and Hoiem, D. Learning without forgetting. *IEEE transactions on pattern analysis and machine intelligence*, 40(12):2935–2947, 2017.

- Liang, Y.-S. and Li, W.-J. Loss decoupling for task-agnostic continual learning. In *Advances in Neural Information Processing Systems*, volume 36, 2024a.
- Liang, Y.-S. and Li, W.-J. InfLoRA: Interference-free low-rank adaptation for continual learning. In *Proceedings of the IEEE/CVF Conference on Computer Vision and Pattern Recognition (CVPR)*, pp. 23638–23647, 2024b.
- Liu, X. and Chang, X. Lora subtraction for drift-resistant space in exemplar-free continual learning. In *Proceedings of the IEEE/CVF conference on Computer Vision and Pattern Recognition*, pp. 15308–15318, 2025.
- Liu, Z., Peng, Y., and Zhou, J. Compositional prompting for anti-forgetting in domain incremental learning. *International Journal of Computer Vision*, 132:5783 – 5800, 2024. URL <https://api.semanticscholar.org/CorpusID:270778693>.
- Lopez-Paz, D. and Ranzato, M. Gradient episodic memory for continual learning, 2022. URL <https://arxiv.org/abs/1706.08840>.
- Malepathirana, T., Senanayake, D., and Halgamuge, S. Napa-vq: Neighborhood-aware prototype augmentation with vector quantization for continual learning. In *Proceedings of the IEEE/CVF International Conference on Computer Vision*, pp. 11674–11684, 2023.
- Mallya, A. and Lazebnik, S. Packnet: Adding multiple tasks to a single network by iterative pruning. In *Proceedings of the IEEE conference on Computer Vision and Pattern Recognition*, pp. 7765–7773, 2018.
- Mallya, A., Davis, D., and Lazebnik, S. Piggyback: Adapting a single network to multiple tasks by learning to mask weights. In *Proceedings of the European Conference on Computer Vision (ECCV)*, pp. 67–82, 2018.
- Masana, M., Liu, X., Twardowski, B., Menta, M., Bagdanov, A. D., and van de Weijer, J. Class-incremental learning: survey and performance evaluation on image classification. *IEEE Transactions on Pattern Analysis and Machine Intelligence*, 45(5):5513–5533, 2022.
- McCloskey, M. and Cohen, N. J. Catastrophic interference in connectionist networks: The sequential learning problem. volume 24 of *Psychology of Learning and Motivation*, pp. 109–165. Academic Press, 1989. doi: [https://doi.org/10.1016/S0079-7421\(08\)60536-8](https://doi.org/10.1016/S0079-7421(08)60536-8). URL <https://www.sciencedirect.com/science/article/pii/S0079742108605368>.
- Moore, R. E., Kearfott, R. B., and Cloud, M. J. *Introduction to interval analysis*. SIAM, 2009.
- Parisi, G. I., Kemker, R., Part, J. L., Kanan, C., and Wermter, S. Continual lifelong learning with neural networks: A review. *Neural Networks*, 113:475–480, 2019.
- Peng, X., Bai, Q., Xia, X., Huang, Z., Saenko, K., and Wang, B. Moment matching for multi-source domain adaptation. In *Proceedings of the IEEE International Conference on Computer Vision*, pp. 1406–1415, 2019.
- Petit, G., Popescu, A., Schindler, H., Picard, D., and Delezoide, B. Fetrl: Feature translation for exemplar-free class-incremental learning. In *Proceedings of the IEEE/CVF winter conference on applications of computer vision*, pp. 3911–3920, 2023.
- Riemer, M., Cases, I., Ajemian, R., Liu, M., Rish, I., Tu, Y., and Tesauro, G. Learning to learn without forgetting by maximizing transfer and minimizing interference. In *International Conference on Learning Representations*, 2018.
- Rusu, A. A., Rabinowitz, N. C., Desjardins, G., Soyer, H., Kirkpatrick, J., Kavukcuoglu, K., Pascanu, R., and Hadsell, R. Progressive neural networks, 2016. arXiv preprint arXiv:1606.04671.
- Rusu, A. A., Rabinowitz, N. C., Desjardins, G., Soyer, H., Kirkpatrick, J., Kavukcuoglu, K., Pascanu, R., and Hadsell, R. Progressive neural networks, 2022. URL <https://arxiv.org/abs/1606.04671>.
- Serrà, J., Surís, D., Miron, M., and Karatzoglou, A. Overcoming catastrophic forgetting with hard attention to the task. In *International Conference on Machine Learning*, pp. 4548–4557, 2018.
- Shi, W. and Ye, M. Prototype reminiscence and augmented asymmetric knowledge aggregation for non-exemplar class-incremental learning. In *Proceedings of the IEEE/CVF International Conference on Computer Vision*, pp. 1772–1781, 2023.
- Shin, H., Lee, J. K., Kim, J., and Kim, J. Continual learning with deep generative replay. In *Advances in neural information processing systems*, volume 30, 2017.
- Smith, J. S., Karlinsky, L., Gutta, V., Cascante-Bonilla, P., Kim, D., Arbelle, A., Panda, R., Feris, R., and Kira, Z. Coda-prompt: Continual decomposed attention-based prompting for rehearsal-free continual learning. In *Proceedings of the IEEE/CVF Conference on Computer Vision and Pattern Recognition (CVPR)*, pp. 11909–11919, 2023. URL <https://arxiv.org/abs/2211.13218>.
- Tang, S., Chen, D., Zhu, J., Yu, S., and Ouyang, W. In *Layerwise optimization by gradient decomposition for continual learning*, pp. 9634–9643, 2021.

- Toldo, M. and Ozay, M. Bring evanescent representations to life in lifelong class incremental learning. In *Proceedings of the IEEE/CVF Conference on Computer Vision and Pattern Recognition*, pp. 16732–16741, 2022.
- Urettini, E. and Carta, A. Online curvature-aware replay: Leveraging 2nd order information for online continual learning. In *International Conference on Machine Learning*, 2025.
- Wang, S., Li, X., Sun, J., and Xu, Z. Training networks in null space of feature covariance for continual learning. In *Proceedings of the IEEE/CVF conference on Computer Vision and Pattern Recognition*, pp. 184–193, 2021.
- Wang, Y., Ma, Z., Huang, Z., Wang, Y., Su, Z., and Hong, X. Isolation and impartial aggregation: A paradigm of incremental learning without interference. In *Proceedings of the AAAI Conference on Artificial Intelligence (AAAI)*, pp. 10209–10217, 2023.
- Wang, Z., Liu, L., Duan, Y., Kong, Y., and Tao, D. Continual learning with lifelong vision transformer. In *Proceedings of the IEEE/CVF Conference on Computer Vision and Pattern Recognition*, pp. 171–181, 2022a.
- Wang, Z., Zhang, Z., Ebrahimi, S., Sun, R., Zhang, H., Lee, C.-Y., Ren, X., Su, G., Perot, V., Dy, J., and Pfister, T. Dualprompt: Complementary prompting for rehearsal-free continual learning. In *European Conference on Computer Vision (ECCV)*, pp. 631–648, 2022b.
- Wang, Z., Zhang, Z., Lee, C.-Y., Zhang, H., Sun, R., Ren, X., Su, G., Perot, V., Dy, J., and Pfister, T. Learning to prompt for continual learning. In *Proceedings of the IEEE/CVF Conference on Computer Vision and Pattern Recognition (CVPR)*, pp. 139–149, 2022c.
- Wołczyk, M., Piczak, K., Wójcik, B., Pustelnik, L., Morawiec, P., Tabor, J., Trzcinski, T., and Spurek, P. Continual learning with guarantees via weight interval constraints. In *International Conference on Machine Learning*, pp. 23897–23911. PMLR, 2022.
- Wortsman, M., Ramanujan, V., Liu, R., Kembhavi, A., Rastegari, M., Yosinski, J., and Farhadi, A. Supermasks in superposition. In *Advances in Neural Information Processing Systems*, volume 33, pp. 15173–15184, 2020.
- Wu, C., Herranz, L., Liu, X., Wang, Y., van de Weijer, J., and Raducanu, B. Memory replay gans: Learning to generate new categories without forgetting. In *Advances in Neural Information Processing Systems*, volume 31, 2018.
- Xu, K., Zou, X., Hua, G., and Zhou, J. Componential prompt-knowledge alignment for domain incremental learning. *ICML*, 2025.
- Yu, L., Twardowski, B., Liu, X., Herranz, L., Wang, K., Cheng, Y., Jui, S., and van de Weijer, J. Semantic drift compensation for class-incremental learning. In *Proceedings of the IEEE/CVF conference on computer vision and pattern recognition*, pp. 6982–6991, 2020.
- Zenke, F., Poole, B., and Ganguli, S. Continual learning through synaptic intelligence, 2017. URL <https://arxiv.org/abs/1703.04200>.
- Zhou, D.-W., Sun, H.-L., Ye, H.-J., and Zhan, D.-C. Expandable subspace ensemble for pre-trained model-based class-incremental learning. In *Proceedings of the IEEE/CVF Conference on Computer Vision and Pattern Recognition*, pp. 23554–23564, 2024.

## A. Extended Overview of Related Works

This section provides an extended literature review of continual learning methods. It first categorizes classical approaches into replay-based, regularization-based, and parameter-isolation techniques. Subsequently, the focus shifts to modern parameter-efficient methods like prompt-based continual learning (e.g., L2P, DualPrompt, CODA-Prompt) and contemporary strategies for managing feature drift in the representation space. Finally, we review recent applications of IA in continual learning, contrasting these ideas with our proposed approach of regularizing functional transformations across model layers.

**Continual Learning.** Continual learning methods (Parisi et al., 2019; De Lange et al., 2021; Masana et al., 2022) can generally be divided into three categories: replay-based, regularization-based, and parameter-isolation-based. *Replay-based* methods employ memory or rehearsal mechanisms to recall past tasks during training, thereby maintaining low loss on those tasks. Two primary strategies are exemplar replay, which stores selected training samples (Chaudhry et al., 2018; Riemer et al., 2018; Chaudhry et al., 2019; Buzzega et al., 2020; Lopez-Paz & Ranzato, 2022; Liang & Li, 2024a; Urettini & Carta, 2025), and generative replay, where models synthesize previous data using generative models (Shin et al., 2017; Wu et al., 2018). *Regularization-based* methods typically introduce a regularization term into the loss function to constrain parameter changes for previously learned tasks. This regularization may be defined by the current task data (Li & Hoiem, 2017; Kim et al., 2023) or previous tasks data (Kirkpatrick et al., 2017; Zenke et al., 2017; Aljundi et al., 2018; Chen et al., 2025) variants. Recent methods limit weight updates to null space of previous data feature covariance (Kong et al., 2022; Tang et al., 2021; Wang et al., 2021; 2022a). Liang & Li (2024a) leverage gradient information from old tasks to construct a subspace for LoRA’s dimensionality reduction matrix, thereby reducing interference between the current task and the previous ones. *Parameter-isolation* methods learn task-specific subnetworks within the model. Techniques such as Progressive Neural Networks (Rusu et al., 2016; 2022), Piggyback (Mallya et al., 2018), PackNet (Mallya & Lazebnik, 2018), HAT (Serrà et al., 2018) and SupSup (Wortsman et al., 2020), ESN (Wang et al., 2023), InfLoRA (Liang & Li, 2024b) allocate and combine parameters for individual tasks. While effective in task-aware settings, these methods are based on assigning test samples to tasks, which may be problematic in some continual learning scenarios.

**Prompt-Based Continual Learning.** These methods are philosophically rooted in parameter-efficient learning, where the vast majority of the model (the backbone) remains unchanged to prevent catastrophic forgetting. The core mechanism involves introducing a small set of new, learnable parameters called *prompts* for each task. These prompts are typically vectors that are prepended to the input sequence embeddings or inserted into intermediate layers. This effectively steers the frozen model’s behavior towards the new task’s objective without overwriting knowledge from previous tasks.

A key innovation in this area is the concept of a *prompt pool*. Rather than learning a single, monolithic prompt for each task, methods like L2P (Wang et al., 2022c) learn a collection of shared prompt vectors. During inference, the model uses a query-based mechanism (e.g., matching input features to prompt keys) to select a sparse combination of prompts from this pool that are most relevant to the current input instance. This approach not only adapts to the current task but also allows the model to potentially recognize and handle inputs from previous tasks by selecting the appropriate “old” prompts, enabling a form of rehearsal-free task routing.

Further refinements focus on the *structure* and *function* of the prompts themselves. For instance, DualPrompt (Wang et al., 2022b) introduced the idea of learning two distinct sets of prompts: a *general* prompt shared across all tasks to capture common knowledge, and a set of *task-specific* prompts to capture task-unique features. CODA-Prompt (Smith et al., 2023) builds on this by using a decomposed attention mechanism, allowing the model to explicitly query general versus task-specific knowledge encoded in the prompts, thereby improving modularity and reducing interference between task-specific instructions. Compositional Prompting (CPrompt; Gao et al. 2024) learns compositional prompt components and promotes their sharing across domains, making it particularly well suited for domain-incremental learning. Consistent Prompting (C-Prompt; Liu et al. 2024) enforces consistency constraints across task-specific prompts, thereby stabilizing representations and mitigating forgetting across tasks.

Despite their success in parameter-efficient, rehearsal-free learning, these methods face a fundamental limitation, particularly in domain-incremental learning (DIL): they struggle to adapt the classifier to distributional shifts between tasks. While the backbone features remain largely fixed, the learned prompts or adapters often fail to capture semantic drift in task labels or decision boundaries. Consequently, when a new task comes from a domain substantially different from previous ones, the classifier may misrepresent the task despite informative backbone features. This highlights the need for future approaches that strategically update classifier parameters or the backbone itself, or develop more flexible prompt-tuning strategies capable of handling evolving task distributions.

**Addressing Feature Drift in Continual Learning.** A critical challenge in continual learning is the feature drift of old classes when new tasks are learned without access to previous samples. Methods often define prototypes of classes (Janson et al., 2022; Goswami et al., 2024a) in the feature space and prevent their drift. SDC (Yu et al., 2020) and (Toldo & Ozay, 2022) estimate and compensate for feature drift with current-task data following each training phase. NAPA-VQ (Malepathirana et al., 2023) and Prototype Reminiscence (Shi & Ye, 2023) reshape old prototypes through topological information with current-data samples. FeTrIL (Petit et al., 2023) introduces a feature translation strategy that aligns new and old class feature distributions. ADC (Goswami et al., 2024b) generates adversarial pseudo-exemplars of new classes to adjust prototypes of earlier classes. EASE (Zhou et al., 2024) introduces a semantic-guided prototype complement strategy that reshapes prototypes of old classes in the feature space adjusted by the current task’s data. Liu & Chang (2025) defines a drift-resistant space in which the model weights can be adjusted to the new task without interfering with old data features. In this work, we do not refer to the concept of prototype. Instead, we mitigate the feature drift by enforcing each layer to preserve its performed transformation on its subdomain defined by the previous tasks’ data.

**Interval Arithmetic in Continual Learning.** Interval arithmetic (Dahlquist & Björck, 2008; Moore et al., 2009) has been applied to continual learning in InterContiNet (Wołczyk et al., 2022), where the key idea is to employ interval constraints on the weights associated with successive tasks. The intersection of these intervals defines the subset of weights that yield satisfactory performance across all tasks. HINT (Krukowski et al., 2025) employs intervals in the embedding space and leverages a hypernetwork to map them to the weight space of the target network. In contrast, we propose a novel approach, also grounded in IA: each layer of the neural network is regularized to preserve its transformation within a subdomain delineated by a hyper-interval, which encapsulates data from previously learned tasks.

**Parameter-Isolation Approaches.** Another strategy is to prevent interference across tasks by isolating parameters. Progressive Neural Networks (Rusu et al., 2022) expand the architecture with task-specific columns and lateral connections, reusing prior knowledge without overwriting it. While this eliminates forgetting by construction, network growth scales linearly with the number of tasks, making these approaches impractical for long task sequences or large-scale settings.

**Regularization-Based Methods.** Regularization-based approaches constrain weight updates to preserve information from earlier tasks. Elastic Weight Consolidation (EWC) (Zenke et al., 2017) introduces a Fisher information–based penalty to protect important parameters, while Synaptic Intelligence (SI) (Li & Hoiem, 2017) and Memory Aware Synapses (MAS) (Kirkpatrick et al., 2017) estimate weight importance through gradient flow. Learning Without Forgetting (LwF) (Aljundi et al., 2018) further anchors predictions of past tasks using knowledge distillation. Despite their success, these methods focus primarily on the parameter space, leaving internal representations vulnerable to drift. As a result, preserving weight importance does not necessarily maintain the functional behavior of learned features.

**Representation-Level Stability.** A complementary direction emphasizes stabilizing learned representations rather than weights. Approaches inspired by interval analysis (Moore et al., 2009) and activation regularization aim to limit representation drift by constraining activations to remain within task-specific bounds. However, these ideas have seen limited adoption in continual learning due to the difficulty of summarizing activation distributions efficiently.

## B. Preliminaries

**Prompt-Based Continual Learning.** Prompt-based continual learning exploits the representational capacity of pretrained ViT (Dosovitskiy et al., 2021) by introducing a small set of learnable parameters (prompts) to adapt the model to new tasks while keeping the backbone frozen. This strategy avoids the computational cost and catastrophic forgetting associated with fine-tuning the entire network.

Formally, consider a ViT encoder  $f_\theta$  with fixed parameters  $\theta$ . The input to the  $l$ -th layer is denoted as  $h^{(l)} \in \mathbb{R}^{L \times D}$ , where  $L$  is the sequence length and  $D$  is the embedding dimension. To adapt the representation, standard approaches employ Prefix-Tuning (Li & Liang, 2021). This mechanism prepends learnable vectors to the internal attention layers. Specifically, learnable prompt matrices  $P_K, P_V \in \mathbb{R}^{L_p \times D}$  (where  $L_p$  is the prompt length) are defined and concatenated with the

standard Key and Value projections:

$$\begin{aligned}
 Q &= h^{(l)}W_Q, \\
 K' &= \left[ P_K; h^{(l)}W_K \right], \\
 V' &= \left[ P_V; h^{(l)}W_V \right], \\
 h^{(l+1)} &= \text{MSA}(Q, K', V'),
 \end{aligned} \tag{15}$$

where MSA denotes Multi-Head Self-Attention,  $[\cdot]$  represents concatenation along the sequence dimension, and  $W_Q, W_K, W_V$  are the frozen projection matrices. In this framework, only the prompts  $P_K, P_V$  and the final classification head are optimized, allowing the system to adapt to non-stationary data streams efficiently.

**Prompt Selection and Memory Structure.** A central challenge in task-agnostic continual learning is selecting appropriate prompts without access to task identifiers at test time. To address this, methods like Learning to Prompt (L2P) (Wang et al., 2022c) maintain a shared prompt pool  $\mathcal{P} = \{(k_i, p_i)\}_{i=1}^M$ , where each learnable prompt  $p_i$  is paired with a key  $k_i \in \mathbb{R}^D$ .

The inference process operates via a content-based retrieval mechanism. First, the input  $x$  is passed through the frozen encoder to generate a query vector  $q(x)$  (typically the  $[\text{CLS}]$  embedding). This query is matched against the stored keys  $\{k_i\}$  using cosine similarity to identify the subset of the  $N$  most relevant prompts. These selected prompts are then explicitly concatenated with the input embeddings or attention prefixes, effectively conditioning the frozen backbone on the retrieved context. During training, optimization is sparse; gradients are applied only to the selected prompt-key pairs, allowing the remaining pool contents to preserve knowledge from disparate tasks.

**Optimization Objective.** Since the discrete retrieval of keys (Top- $K$ ) is non-differentiable, gradients cannot backpropagate to the prompt pool directly. Consequently, prompt-based methods typically minimize a composite objective  $\mathcal{L}_{\text{Total}} = \mathcal{L}_{\text{task}} + \lambda \mathcal{L}_{\text{match}}$ . Here,  $\mathcal{L}_{\text{task}}$  (e.g., Cross-Entropy) updates the prompts and classifier head, while the surrogate loss  $\mathcal{L}_{\text{match}}$  pulls the keys  $\{k_i\}$  closer to the queries of their assigned inputs, ensuring that the retrieval mechanism aligns with the data distribution.

**Hierarchical and Decomposed Prompting.** DualPrompt (Wang et al., 2022b) decouples plasticity and stability by partitioning the prompts into distinct functional groups: G-Prompts ( $g$ ) for task-invariant features and E-Prompts ( $e_t$ ) for task-specific experts. These are inserted into complementary depths of the backbone:

$$h^{(l+1)} = \begin{cases} \text{MSA}(h^{(l)}, e_t) & \text{if } l \leq L_e \quad (\text{Expert Layers}) \\ \text{MSA}(h^{(l)}, g) & \text{if } l > L_e \quad (\text{General Layers}) \end{cases} \tag{16}$$

where  $e_t$  is retrieved via a task-specific key  $k_t$ .

CODA-Prompt (Smith et al., 2023) generalizes this by replacing discrete selection with a soft, weighted summation of components. The input query  $q(x)$  attends to the entire pool  $\mathcal{P} = \{P_m\}_{m=1}^M$  via a learnable attention mechanism:

$$\alpha_m(x) = \text{Softmax} \left( \frac{\langle q(x) \odot A_m, K_m \rangle}{\tau} \right), \quad p(x) = \sum_{m=1}^M \alpha_m(x) P_m. \tag{17}$$

Here,  $A_m$  is a query-modulation vector and  $\odot$  denotes the Hadamard product. This differentiable formulation allows the prompt  $p(x)$  to form complex linear combinations of existing knowledge, stabilized by an orthogonality penalty on the keys to minimize inter-component redundancy.

## C. Implementation Details

**Architecture and Training.** All experiments utilize a ViT-B/16 backbone (Dosovitskiy et al., 2021) pre-trained on ImageNet-21k. Consistent with standard prompt-learning protocols, the backbone parameters remain frozen to ensure stable feature extraction. Adaptation is achieved exclusively by optimizing the injected prompts and the shared classification head. Since we focus on DIL, the label space remains constant across all tasks; thus, the final classifier output dimension is fixed, and no task-specific masking is required. The primary optimization challenge is adapting to distributional shifts while preserving the shared decision boundaries.

**Datasets and Protocols.** We evaluate InTAct on four benchmarks designed to assess robustness against varying degrees of domain shift: **DomainNet** (Peng et al., 2019) offers the most severe visual shifts, consisting of six distinct domains (Clipart, Infograph, Painting, Quickdraw, Real, Sketch). In our DIL setting, each domain constitutes a separate task, processed sequentially. **ImageNet-R** (Hendrycks et al., 2021) contains 200 classes rendered in diverse artistic styles (e.g., cartoons, embroidery). To construct a DIL sequence, we partition the dataset into 15 sequential tasks, ensuring all classes are present in every task but represented by different samples/styles. **ImageNet-C** (Hendrycks & Dietterich, 2019) evaluates robustness against corruption. Following the protocol of (Liu et al., 2024), we utilize the 200 classes overlapping with ImageNet-R, subjecting them to 15 types of algorithmic perturbations (e.g., blur, noise) to form the task sequence. Finally, **ImageNet-Mix** (Liu et al., 2024) combines the styles of ImageNet-R with the corruptions of ImageNet-C, resulting in a 30-task benchmark that rigorously tests stability under compound distributional shifts.

All datasets are normalized and transformed during both training and evaluation, following the KA-Prompt method (Xu et al., 2025).

**Code and Reproducibility.** For experiments involving prompt-based architectures, we build directly on the official implementation of CODA-Prompt, and we adapt the DomainNet DIL task handlers from the KA-Prompt GitHub repository. To ensure strict reproducibility and a fair comparison with reported baselines, we match the software environment used in CODA-Prompt, including the same `timm` version (0.9.7), which is essential to ensure identical pretrained ViT weights. Our method InTAct is integrated into the CODA-Prompt codebase without modifying the underlying prompt selection or training routines.

All experiments were conducted on NVIDIA H100 (80GB), A100 (40GB) and V100 (32GB) GPUs within a DGX cluster, as well as on standalone RTX 4090 (32 GB) machines. Full training pipelines, configuration files, and scripts for reproducing all reported results are available in our GitHub repository.

## D. Hyperparameter Configuration

To ensure fair comparison, we integrate InTAct into the CODA-Prompt framework using identical backbone and prompt configurations as the baseline. We fix  $\lambda_{\text{align}} = 1$ , while determining the optimal coefficients for the remaining regularizers via grid search over the ranges  $\lambda_{\text{var}} \in \{10^{-3}, \dots, 1.0\}$  and  $\lambda_{\text{IntDrift}}, \lambda_{\text{Feat}} \in \{10^{-6}, \dots, 10^{-1}\}$ . The specific values selected for the final evaluation are detailed in Table 3.

Table 3. **Optimal Hyperparameters.** Selected hyperparameters for InTAct across different benchmarks.

Dataset	$\lambda_{\text{Feat}}$	$\lambda_{\text{IntDrift}}$	$\lambda_{\text{Var}}$
DomainNet	$10^{-4}$	$10^{-3}$	1.0
ImageNet-R	$10^{-1}$	$10^{-3}$	$10^{-1}$
ImageNet-C	$10^{-1}$	$10^{-4}$	$10^{-1}$
ImageNet-Mix	$10^{-1}$	$10^{-4}$	$10^{-1}$

## E. Interval Arithmetic

IA, introduced in its modern form by Ramon E. Moore (Moore et al., 2009), provides a method for performing computations on ranges of real numbers rather than single point values. An interval  $x$  is a closed, bounded set of real numbers defined by its endpoints,  $x = [x_l, x_u]$ , such that  $x_l \leq x_u$ . This framework is essential for validated numerics, as it allows for the rigorous containment of numerical errors, including rounding errors and uncertainties in initial data.

### E.1. Fundamental Operations

The fundamental principle of IA is the *inclusion property*: the resulting interval of an operation must contain all possible results from applying the same operation to any real numbers within the operand intervals. Let  $x = [x_l, x_u]$  and  $y = [y_l, y_u]$  be two intervals. The elementary arithmetic operations are defined as follows:

**Addition.** The sum is obtained by adding the respective endpoints:

$$x + y = [x_l + y_l, x_u + y_u] \tag{18}$$

**Subtraction.** The difference is computed by cross-adding the endpoints:

$$x - y = [x_l - y_u, x_u - y_l] \tag{19}$$

**Multiplication.** The product is the interval spanning the minimum and maximum of the four products of the endpoints.

$$x \cdot y = [z_l, z_u], \tag{20}$$

where

$$z_l = \min(x_l y_l, x_l y_u, x_u y_l, x_u y_u), \tag{21}$$

$$z_u = \max(x_l y_l, x_l y_u, x_u y_l, x_u y_u). \tag{22}$$

**Division.** Division is defined as multiplication by the reciprocal of  $y$ , provided that  $0 \notin y$ .

$$\frac{x}{y} = x \cdot \left[ \frac{1}{y_u}, \frac{1}{y_l} \right], \quad \text{if } 0 \notin [y_l, y_u]$$

Suppose the divisor interval  $y$  contains zero. In that case, the operation is typically undefined or results in extended intervals (e.g., a union of two intervals), depending on the specific framework being used (Moore et al., 2009).

## E.2. Interval Matrix Multiplication

The operations of IA extend naturally to linear algebra, enabling computations with interval matrices. An interval matrix  $A$  is a matrix whose elements are intervals. Given two compatible interval matrices,  $A$  and  $B$ , their product  $C = AB$  is an interval matrix where each element  $c_{ij}$  the interval extension of the standard dot product defines:

$$c_{ij} = \sum_{k=1}^n a_{ik} b_{kj}. \tag{23}$$

Here, each multiplication  $a_{ik} b_{kj}$  is an interval multiplication, and the summation  $\sum$  represents a sequence of interval additions. This operation is fundamental for solving interval linear systems, which are crucial for analyzing the effects of bounded uncertainties in models. However, this definition is highly susceptible to the dependency problem; if the same interval variable appears in multiple entries of  $A$  or  $B$ , the resulting bounds on  $C$  can be much wider than the true range.

## E.3. Interval Convolutions

IA can be extended to operations like convolutions, which are fundamental in areas such as signal processing and image analysis. By representing an input signal  $X$  and a filter kernel  $W$  as intervals, one can analyze systems where inputs or parameters are subject to bounded uncertainties.

A key operation is the interval convolution. For a 2D input  $X$ , an interval kernel (filter)  $W$ , and an optional interval bias  $b$ , the resulting output feature map  $Y$  is computed as:

$$Y_{ij} = \left( \sum_{k,l} X_{i+k,j+l} \cdot W_{k,l} \right) + b. \tag{24}$$

This computation propagates the interval bounds through the filtering operation, producing a rigorous enclosure for the true output. This is particularly useful in robust state estimation and control, where system parameters or measurements are known to lie within certain bounds (Jaulin et al., 2001).

## E.4. Properties and Practical Considerations

While IA provides a mechanism for bounding activations, two characteristics are notable for implementation.

First, theoretically, IA requires *directed rounding*, expanding the bounds slightly outward, to strictly guarantee that no precision errors are excluded. However, in the context of neural networks, these microscopic floating-point errors are negligible compared to the inherent high variance and noise of the feature activations.

Second, IA is subject to the *dependency problem*. When a variable appears multiple times in an expression, each occurrence is treated independently, leading to an overestimation of the true range (often called the *wrapping effect*). For example, computing  $x - x$  for  $x \in [0, 1]$  yields  $[-1, 1]$  rather than the true set  $\{0\}$ . In our framework, this results in conservative (looser) bounds. While this guarantees that no valid data is excluded, it implies that the protected hypercubes may occupy more volume than the underlying data strictly requires.

## F. Metrics

We assess continual learning performance using AA. Let  $N$  be the total number of tasks, and  $R_{i,j}$  denote the test accuracy on task  $i$  after the model has finished training on task  $j$ . Average Accuracy (AA) reports the mean performance across all tasks after the final training session:

$$AA = \frac{1}{N} \sum_{i=1}^N R_{i,N}. \quad (25)$$

## G. Detailed Derivation of Internal Representation Drift Loss

In this section, we provide the step-by-step derivation of the regularization term  $\mathcal{L}_{\text{IntDrift}}$ . Our goal is to ensure that the parameter updates for a layer do not alter the layer’s output for any input belonging to the *established activation region* of previous tasks.

**The Stability Condition.** Consider the  $l$ -th affine layer of the network with weights  $W_l$  and bias  $b_l$ . Let  $h \in \mathbb{R}^{D_{in}}$  denote the input to this layer (i.e., the output of layer  $l - 1$ ). The preactivation output is given by:

$$f(h; \theta_l) = W_l h + b_l. \quad (26)$$

After training on a new task, the parameters update to  $W_l + \Delta W_l$  and  $b_l + \Delta b_l$ . The drift in the preactivation for a given input  $h$  is:

$$\delta(h) = f(h; \theta_l + \Delta \theta_l) - f(h; \theta_l) = \Delta W_l h + \Delta b_l. \quad (27)$$

To prevent catastrophic forgetting, we require this drift to be zero for all inputs residing within the hypercube  $\mathcal{H}$  defined by the previous tasks. Let this hypercube be denoted by the interval vector  $[\underline{h}, \bar{h}]$ . The condition is:

$$\Delta W_l h + \Delta b_l = 0, \quad \forall h \in [\underline{h}, \bar{h}]. \quad (28)$$

**Interval Extension.** Since checking every point  $h$  is impossible, we use IA to bound the drift  $\delta(h)$ . The interval extension of the linear map  $\Delta W_l h$  computes the tightest box containing the image of the input hypercube. For the  $i$ -th output coordinate, the drift bounds  $[\underline{\delta}_i, \bar{\delta}_i]$  are computed as:

$$[\underline{\delta}_i, \bar{\delta}_i] = \Delta W_{l,i} [\underline{h}, \bar{h}] + \Delta b_{l,i}, \quad (29)$$

where  $\Delta W_{l,i}$  is the  $i$ -th row of the update matrix.

**Decomposition into Positive and Negative Parts.** In IA, the product of a scalar  $w$  and an interval  $[a, b]$  depends on the sign of  $w$ :

$$w \cdot [a, b] = \begin{cases} [wa, wb] & \text{if } w \geq 0 \\ [wb, wa] & \text{if } w < 0 \end{cases}. \quad (30)$$

To vectorize this operation, we decompose the weight row  $\Delta W_{l,i}$  into its positive and negative components:

$$\Delta W_{l,i}^+ = \max(0, \Delta W_{l,i}), \quad \Delta W_{l,i}^- = \max(0, -\Delta W_{l,i}). \quad (31)$$

Thus,  $\Delta W_{l,i} = \Delta W_{l,i}^+ - \Delta W_{l,i}^-$ . Applying this to the interval product:

$$\Delta W_{l,i} [\underline{h}, \bar{h}] = (\Delta W_{l,i}^+ - \Delta W_{l,i}^-) [\underline{h}, \bar{h}] \quad (32)$$

$$= \underbrace{\Delta W_{l,i}^+ [\underline{h}, \bar{h}]}_{\text{Preserves Order}} - \underbrace{\Delta W_{l,i}^- [\underline{h}, \bar{h}]}_{\text{Reverses Order (handled by subtraction)}} \quad (33)$$

$$= [\Delta W_{l,i}^+ \underline{h}, \Delta W_{l,i}^+ \bar{h}] - [\Delta W_{l,i}^- \underline{h}, \Delta W_{l,i}^- \bar{h}]. \quad (34)$$

Using the interval subtraction rule  $[a, b] - [c, d] = [a - d, b - c]$ , we derive the bounds for the drift:

$$\underline{\delta}_i = \Delta W_{l,i}^+ \underline{h} - \Delta W_{l,i}^- \bar{h} + \Delta b_{l,i}, \quad (35)$$

$$\bar{\delta}_i = \Delta W_{l,i}^+ \bar{h} - \Delta W_{l,i}^- \underline{h} + \Delta b_{l,i}. \quad (36)$$

**Loss Formulation.** The condition  $\delta(h) = 0$  implies that the interval  $[\underline{\delta}_i, \bar{\delta}_i]$  must collapse to  $[0, 0]$ . We enforce this by minimizing the squared  $L_2$  norm of the bounds across the set of indices corresponding to the protected layers, denoted as  $\mathcal{S}$ :

$$\mathcal{L}_{\text{IntDrift}} = \sum_{l \in \mathcal{S}} \sum_i (\|\underline{\delta}_{l,i}\|^2 + \|\bar{\delta}_{l,i}\|^2). \quad (37)$$

Minimizing this term compresses the drift range, ensuring the updated model behaves identically to the old model within the protected regions.

## H. Internal Representation Drift for Convolutional Layers

**Convolutional Layer.** We extend the derivation of  $\mathcal{L}_{\text{IntDrift}}$  to 2D convolutional layers. Let  $f(h; \theta_l) = \text{Conv2d}(h, W_l) + b_l$  denote the layer operation. Since convolution is a linear operator applied to local spatial patches, it can be reformulated as an affine transformation on unfolded input vectors.

Consider a single output channel  $i$ . The preactivation at a specific spatial location is computed by the dot product of the flattened filter kernel  $k_i$  (derived from  $W_l$ ) and the corresponding flattened input patch  $h_p$ . Let  $\Delta k_i$  and  $\Delta b_i$  represent the parameter updates. The stability condition requires the drift to be zero for any patch  $h_p$  within the established bounds  $[\underline{h}_p, \bar{h}_p]$ :

$$\Delta k_i^\top h_p + \Delta b_i = 0, \quad \forall h_p \in [\underline{h}_p, \bar{h}_p]. \quad (38)$$

By treating the flattened patch  $h_p$  as the input vector, this formulation becomes mathematically identical to the affine case derived in Appendix G. We apply the same IA decomposition. Let  $\Delta k_i^+$  and  $\Delta k_i^-$  denote the positive and negative components of the filter update. The bounds on the drift  $[\underline{\delta}_i, \bar{\delta}_i]$  for this channel are:

$$\underline{\delta}_i = \Delta k_i^+ \underline{h}_p - \Delta k_i^- \bar{h}_p + \Delta b_i, \quad (39)$$

$$\bar{\delta}_i = \Delta k_i^+ \bar{h}_p - \Delta k_i^- \underline{h}_p + \Delta b_i. \quad (40)$$

The loss  $\mathcal{L}_{\text{IntDrift}}$  is then computed by minimizing the squared  $L_2$  norm of these bounds, summed across all channels and spatial locations. This ensures that the convolutional filters remain functionally invariant within the protected local geometric regions of past tasks.

**Batch Normalization Layer.** During inference, a Batch Normalization (BN) layer operates as a channel-wise affine transformation. Let  $\gamma, \beta$  be the learnable parameters and  $\mu, \sigma^2$  be the frozen running statistics. The layer operation is:

$$f(h; \theta) = \underbrace{\frac{\gamma}{\sqrt{\sigma^2 + \epsilon}}}_{W_{\text{eff}}} h + \underbrace{\left( \beta - \frac{\gamma \mu}{\sqrt{\sigma^2 + \epsilon}} \right)}_{b_{\text{eff}}}. \quad (41)$$

When the parameters update by  $(\Delta\gamma, \Delta\beta)$ , the resulting functional drift is equivalent to an affine update with effective parameters:

$$\Delta W_{\text{eff}} = \frac{\Delta\gamma}{\sqrt{\sigma^2 + \epsilon}}, \quad \Delta b_{\text{eff}} = \Delta\beta - \frac{\Delta\gamma \mu}{\sqrt{\sigma^2 + \epsilon}}. \quad (42)$$

Since the drift form  $\Delta W_{\text{eff}} h + \Delta b_{\text{eff}}$  is identical to the standard affine case, we compute  $\mathcal{L}_{\text{IntDrift}}$  directly using the interval bounds derived in Appendix G, substituting  $\Delta W_l$  and  $\Delta b_l$  with  $\Delta W_{\text{eff}}$  and  $\Delta b_{\text{eff}}$ .

## I. Training Algorithm

The complete training procedure for InTAct is detailed in Algorithm 1.

**Optimization Setup.** We optimize the set of learnable parameters  $\Psi = \{\phi, \mathbf{w}\}$ , comprising the prompt pool parameters  $\phi$  and the classifier weights  $\mathbf{w}$ , while keeping the backbone  $f(\cdot; \theta)$  frozen. The training process incorporates a standard prompt-query mechanism QUERYPROMPTS that retrieves task-relevant prompts and computes any method-specific auxiliary losses (e.g., orthogonality penalties), denoted as  $\mathcal{L}_{\text{aux}}$ .

**Training Dynamics.** The optimization strategy gradually balances stability and adaptability across tasks. During the first task ( $t = 1$ ), the model optimizes the classification loss together with the variance regularization  $\mathcal{L}_{\text{Var}}$ , which is crucial for compressing early task activations into compact, well-defined regions. For subsequent tasks ( $t \geq 2$ ), the full regularization is applied by incorporating  $\mathcal{L}_{\text{IntDrift}}$  and  $\mathcal{L}_{\text{Align}}$ . These terms encourage the model to produce consistent outputs for previously seen data, ensuring that new learning does not interfere with the predictions established for earlier tasks.

---

### Algorithm 1 InTAct Training Procedure

---

**Require:** Sequence of  $T$  tasks  $\{\mathcal{D}_t\}_{t=1}^T$ , Frozen backbone  $f_\theta$ .  
**Require:** Learnable classification head  $g(\cdot; \mathbf{w})$  and prompts  $\phi$ .  
**Require:** Learning rate  $\eta$ , Hyperparameters  $\{\lambda_{\text{Var}}, \lambda_{\text{IntDrift}}, \lambda_{\text{Feat}}, \lambda_{\text{Prompt}}, \alpha\}$ .  
**Ensure:** Optimized parameters  $\Psi = \{\phi, \mathbf{w}\}$ .

- 1: **Initialize:**  $\mathcal{S}$  as the subset of layers for hypercube tracking;  $\mathcal{H}_l \leftarrow \emptyset$  for all  $l \in \mathcal{S}$ .
- 2: **for** task  $t = 1$  to  $T$  **do**
- 3:   **for** epoch  $e = 1$  to  $E$  **do**
- 4:     **for** batch  $(x, y) \sim \mathcal{D}_t$  **do**
- 5:        $x_p, \mathcal{L}_{\text{aux}} \leftarrow \text{QUERYPROMPTS}(x)$  {Retrieve task-specific prompts}
- 6:        $z \leftarrow f_\theta(x_p)$  {Representation from backbone}
- 7:        $\hat{y} \leftarrow g(z; \mathbf{w})$  {Forward pass through classification head}
- 8:        $\mathcal{L}_{\text{Total}} \leftarrow \mathcal{L}_{\text{CE}}(y, \hat{y}) + \lambda_{\text{Prompt}}\mathcal{L}_{\text{aux}} + \lambda_{\text{Var}}\mathcal{L}_{\text{Var}}$
- 9:       **if**  $t > 1$  **then**
- 10:           $\mathcal{L}_{\text{stab}} \leftarrow \lambda_{\text{Feat}}\mathcal{L}_{\text{Feat}} + \lambda_{\text{IntDrift}}\mathcal{L}_{\text{IntDrift}} + \mathcal{L}_{\text{Align}}$
- 11:           $\mathcal{L}_{\text{Total}} \leftarrow \mathcal{L}_{\text{Total}} + \mathcal{L}_{\text{stab}}$
- 12:       **end if**
- 13:        $\Psi \leftarrow \Psi - \eta \nabla_{\Psi} \mathcal{L}_{\text{Total}}$
- 14:     **end for**
- 15:   **end for**
- 16:   **Update Cumulative Hypercube:**
- 17:   **for** each layer  $l \in \mathcal{S}$  **do**
- 18:      $[\underline{v}, \bar{v}] \leftarrow \text{PercentileBounds}(h_l(x_p), \alpha)$  {Compute bounds for current task}
- 19:     **if**  $\mathcal{H}_l = \emptyset$  **then**
- 20:        $\mathcal{H}_l \leftarrow [\underline{v}, \bar{v}]$
- 21:     **else**
- 22:        $\mathcal{H}_l \leftarrow \mathcal{H}_l \cup [\underline{v}, \bar{v}]$  {Expand hypercubes via interval union}
- 23:     **end if**
- 24:   **end for**
- 25: **end for**

---

## J. InTAct in other prompt-based methods

Table 4 reports the performance of our method on the DomainNet and ImageNet-R benchmarks. We adopt the optimal hyperparameter settings for the Class-Incremental Learning (CIL) scenario as identified in the comprehensive CODA-Prompt study (Smith et al., 2023), applying them consistently to both the baseline methods and our integrated approach. InTAct acts as a modular enhancement, seamlessly augmenting existing frameworks such as L2P and DualPrompt. As shown in the results, this integration leads to substantial improvements: on the challenging ImageNet-R benchmark, InTAct increases the AA of L2P by +8.0 p.p. and of DualPrompt by +8.5 p.p. Comparable gains are observed on DomainNet, demonstrating that InTAct effectively improves the plasticity-stability trade-off. Note that these experiments used a different version of the `timm` library than Table 1; as a result, while relative gains are consistent, absolute performance values are not directly comparable across tables.

## K. Additional Visualization

**Internal Representation Stability.** We analyze the stability of internal representations using the Split-MNIST benchmark in the DIL scenario. For this experiment, we apply InTAct to a standard Multi-Layer Perceptron (MLP). To align with our

Table 4. Performance results of integrating InTAct with L2P and DualPrompt. We report AA for ImageNet-R and DomainNet in the DIL setting. Incorporating InTAct consistently yields performance gains over prompt-based baselines. Results are averaged over 5 random seeds.

Method	DomainNet	ImageNet-R	Average
L2P	48.44±0.09	50.34±0.26	49.39±0.18
<b>+ InTAct</b>	<b>53.44±0.02</b>	<b>58.34±0.24</b>	<b>55.89±0.13</b>
DualPrompt	50.87±0.31	53.31±0.36	52.09±0.34
<b>+ InTAct</b>	<b>56.83±0.28</b>	<b>61.85±0.45</b>	<b>59.34±0.37</b>

framework, we treat the first hidden layer as the fixed feature extractor (applying  $\mathcal{L}_{\text{Feat}}$  to its outputs) and apply the rest of regularization terms ( $\mathcal{L}_{\text{IntDrift}}$ ,  $\mathcal{L}_{\text{Var}}$ ,  $\mathcal{L}_{\text{Align}}$ ) to the subsequent trainable layers.

Fig. 6 quantifies the *internal representation drift* experienced by historical data as the model adapts to new tasks. We track the normalized  $L_1$  difference between the activations of reference samples at the end of their initial training task and their activations after subsequent tasks. While our baseline (LwF) exhibits progressive drift, indicating that the internal features of old data are being distorted by new plasticity, InTAct effectively bounds these changes, maintaining the geometric integrity of the latent space throughout the learning sequence.

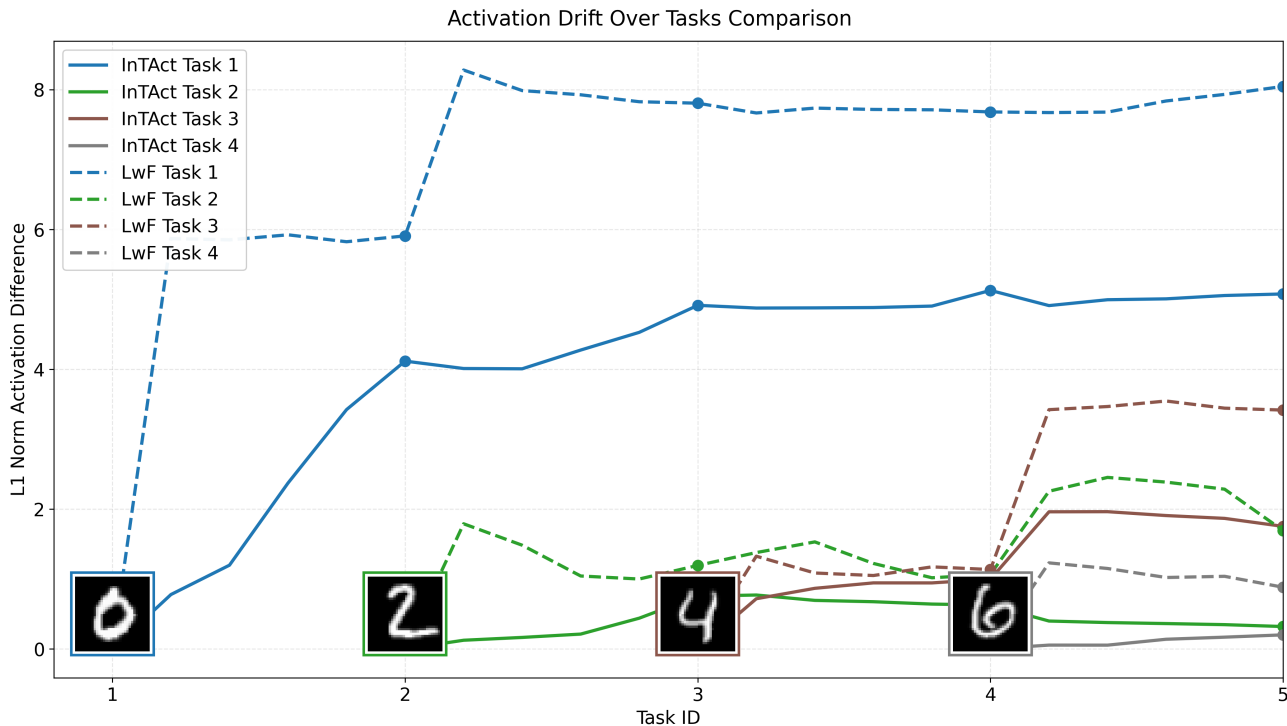


Figure 6. Evolution of Internal Drift. Activation stability on Split-MNIST (DIL). The plot tracks the cumulative  $L_1$  shift in hidden activations for reference images from early tasks as the model trains on later tasks. InTAct successfully suppresses drift compared to LwF, validating the effectiveness of the proposed regularization.

**Conclusions.** The comparative analysis reveals a fundamental difference in plasticity management. The baseline (LwF) exhibits unbounded, cumulative drift; as the sequence progresses, the feature representations of early tasks are continuously distorted by new updates, leading to the erosion of historical knowledge. In contrast, InTAct effectively saturates this drift. After a minor initial adaptation phase (attributable to the necessary expansion of the shared decision boundary), the activation shifts plateau. This confirms that the drift-prevention mechanism successfully locks the functional geometry of the network for past tasks, preventing the "feature erasure" typically associated with catastrophic forgetting.

## L. Parameters and Overhead Comparison

Table 5 presents a comparison of computational efficiency on ImageNet-R (NVIDIA RTX 4090), using reference metrics from (Xu et al., 2025) for state-of-the-art baselines. Our implementation of the whole model has a slightly higher base parameter count (3.99 M vs 2.64 M) due to modified hyperparameters (e.g., prompt pool size).

InTAct introduces **zero additional learnable parameters** beyond this baseline while delivering substantial performance improvements. The method requires 18.04 GB of GPU memory and 0.51 s per batch, which is highly competitive compared to other approaches. For instance, InTAct uses less than half the memory of CPrompt (41.6 GB) and achieves faster inference than retrieval-intensive KA-Prompt (0.72 s per batch). These results demonstrate that InTAct combines state-of-the-art accuracy with efficient memory usage and high throughput, making it both practical and scalable for continual learning on large-scale benchmarks.

Table 5. Efficiency comparison on ImageNet-R. We report the total parameters, trainable parameters, GPU memory usage, and batch inference time. Based on (Xu et al., 2025).

Methods	Total Params	Trainable Params	GPU Memory (GB)	Batch time (S)	Avg-ACC
L2P	86,263,843	311,387	19.33	0.66	56.55±0.33
S-Prompts	92,964,094	1,637,910	14.90	0.39	27.23±0.16
DualPrompt	86,514,211	561,755	19.45	0.66	59.47±1.00
CODA-Prompt	88,437,580	2,638,926	19.18	0.80	55.21±0.33
CPrompt	92,485,224	2,689,168	41.64	1.18	59.48±1.09
C-Prompt	89,180,505	3,381,851	11.99	0.42	62.43±0.49
KA-Prompt	89,180,505	3,381,851	19.28	0.72	66.51±0.36
<b>InTAct (Ours)</b>	89,792,456	3,993,800	18.04	0.51	<b>74.23±0.16</b>